HHS Public Access

Author manuscript

Bone. Author manuscript; available in PMC 2023 September 21.

Published in final edited form as:

Bone. 2023 April ; 169: 116682. doi:10.1016/j.bone.2023.116682.

Antibodies to sclerostin or G-CSF receptor partially eliminate bone or marrow adipocyte loss, respectively, following vertical sleeve gastrectomy

Ziru Li[1,2,#], **Kevin Qiu**[1,#], **Jingtong Zhao**[1], **Katrina Granger**[1], **Hui Yu**[1], **Alfor G. Lewis**[3], **Andriy Myronovych**[3], **Mouhamadoul H. Toure**[3], **Sarah J. Hatsell**[4], **Aris N. Economides**[4], **Randy J. Seeley**[3], **Ormond A. MacDougald**[1,5,*]

[1]University of Michigan Medical School, Department of Molecular & Integrative Physiology, Ann Arbor, MI

[2]MaineHealth Institute for Research, Scarborough, ME

[3]University of Michigan Medical School, Department of Surgery, Ann Arbor, MI

[4]Regeneron Pharmaceuticals Inc, Tarrytown, NY

[5]University of Michigan Medical School, Department of Internal Medicine, Ann Arbor, MI

Abstract

Vertical sleeve gastrectomy (VSG), the most utilized bariatric procedure in clinical practice, greatly reduces body weight and improves a variety of metabolic disorders. However, one of its long-term complications is bone loss and increased risk of fracture. Elevated circulating sclerostin (SOST) and granulocyte-colony stimulating factor (G-CSF) concentrations have been considered as potential contributors to VSG-associated bone loss. To test these possibilities, we administrated antibodies to SOST or G-CSF receptor and investigated alterations to bone and marrow niche following VSG. Neutralizing either SOST or G-CSF receptor did not alter beneficial effects of VSG on adiposity and hepatic steatosis, and anti-SOST treatment provided a further improvement to glucose tolerance. SOST antibodies partially reduced trabecular and cortical bone loss following VSG by increasing bone formation, whereas G-CSF receptor antibodies had no effects on bone mass. The expansion in myeloid cellularity and reductions in bone marrow adiposity seen with VSG were partially eliminated by treatment with Anti-G-CSF receptor. Taken together, these experiments demonstrate that antibodies to SOST or G-CSF receptor may act

[*]**Correspondence to:** Ormond A. MacDougald, North Campus Research Complex, 2800 Plymouth Road, Building 25, Office 3686, Ann Arbor, Michigan 48109, macdouga@umich.edu.
[#]Authors contributed equally to this work.

Conflict of interest statement

RJS has received research support from Novo Nordisk, AstraZeneca and Fractyl. RJS has served as a paid consultant to Novo Nordisk, Scohia, CinRx, Structure Therapeutics and has equity in Calibrate and Rewind. SJH and ANE hold stock in Regeneron. OAM has received grant support from Regeneron Pharmaceuticals, Inc., CombiGene AB, and Rejuvenate Bio. All other authors have declared that no conflicts of interest exist.

Credit authorship contribution statement

ZL, KQ, RJS and OAM conceived the studies and planned the experimental design. SJH and ANE provided antibodies and approved the experimental design. ZL, KQ, KG, AL, AM, and MT performed the experiments. ZL, KQ, KG, EZ, HY and OAM analyzed the data. ZL and OAM wrote the manuscript, whilst all other authors edited and approved the final manuscript.

through independent mechanisms to partially block effects of VSG on bone loss or marrow niche cells, respectively.

Keywords

Vertical sleeve gastrectomy; bone loss; sclerostin; SOST; G-CSF receptor; bone marrow adipose tissue

1. Introduction

Obesity is a prevalent health concern that contributes to other detrimental conditions such as cardiovascular diseases and type 2 diabetes. Treatment of obese individuals primarily revolves around weight management through diet and exercise, but in cases of severe obesity, the use of various bariatric surgical approaches is gaining popularity for significantly reducing body weight [1] and ameliorating type 2 diabetes [2, 3]. Unfortunately, bariatric surgeries are also associated with adverse side effects, including bone loss and increased fracture risk [4–6]. Investigation of the mechanisms underlying bariatric surgery-induced bone loss is essential, as these insights have potential to uncover novel therapeutic targets. The most commonly performed bariatric surgery is vertical sleeve gastrectomy (VSG), which removes a significant portion of the stomach along the greater curvature. Using a mouse model, our previous work found that VSG causes trabecular and cortical bone loss due to impaired osteoid mineralization and bone formation [7].

Osteocytes comprise 90% of the cells in bone, and are considered to be the ‘command and control’ for skeletal remodeling. Sclerostin (SOST) is a secretory product of osteocytes that travels through canalicular networks to reach bone surfaces where sclerostin inhibits WNT signaling to reduce osteoblastogenesis and accelerate osteoclastogenesis [8, 9]. Clinical literature suggests that sclerostin is elevated in human patients after bariatric surgery and is correlated with bone loss [5, 10]. Inhibition of sclerostin with specific antibodies has been extensively analyzed in mouse models and humans as a therapy for combating bone losses in response to estrogen-depletion [11, 12], age [13], hyperthyroidism [14], disuse [15], and myeloma [16, 17]. However, anti-sclerostin (Anti-SOST) monoclonal antibodies have not been evaluated for their potential to prevent bone loss following VSG.

In mice, VSG also has profound effects on the bone marrow niche, including loss of bone marrow adipose tissue (BMAT) and expansion of myeloid cellularity, leading to increased circulating neutrophils [7]. To delineate factors mediating effects of VSG on bone and the marrow niche, we found that circulating granulocyte-colony stimulating factor (G-CSF) was increased in both mice and young female VSG patients. Elevation of circulating G-CSF recapitulated many effects of VSG on bone and the marrow niche, including loss of bone, expansion of myelopoiesis and depletion of marrow adipocytes. In mice lacking G-CSF, effects of VSG on BMAT depletion and myeloid expansion were reduced, but did not ameliorate VSG-induced bone loss, suggesting G-CSF plays an intermediary role for some effects of VSG on the bone marrow niche. Since G-CSF is a factor integral to development of these negative effects of VSG on bone and marrow niche, we investigated whether blocking the G-CSF receptor (GCSFR) would alleviate negative side effects.

Our results demonstrate that antibody treatment targeting SOST or GCSFR did not interfere with the beneficial effects of VSG to reduce fat mass and hepatosteatosis; anti-SOST even contributed a further improvement of glucose homeostasis. Furthermore, Anti-SOST treatment substantially increased trabecular and cortical bone. However, the increase in endocortical bone formation only partially rescued losses of bone mass and mechanical strength following VSG. Blocking G-CSF receptor did not influence bone mass, but VSG-induced myeloid expansion was largely eliminated and BMAT depletion was diminished. In summary, antibodies to SOST and G-CSF receptor act through distinct mechanisms to partially block effects of VSG on bone or the marrow niche. Further studies will be required to identify cellular therapeutic targets of SOST and G-CSF in osteocytes, osteoblasts, bone marrow adipocytes, and/or other hematopoietic cell populations.

2. Material and Methods

2.1 Animals

C57BL/6J male mice were obtained from the Jackson Laboratory at six weeks of age. Mice were housed on a 12-hour light/dark cycle in the Unit for Laboratory Animal Medicine at the University of Michigan. Mice were provided *ad libitum* access to high-fat diet (HFD; 60% calories from fat, D12492; Research Diets) for eight weeks prior to surgery to induce obesity, and for the four weeks following surgery.

2.2 Vertical sleeve gastrectomy

Obese C57BL/6J mice were randomly assigned into VSG and Sham groups. The VSG surgery used an Echelon-Flex 35 Powered Stapler (Ethicon Endo-Surgery, USA) to resect the lateral ~60% of the stomach, leaving a tubular gastric remnant in continuity with the proximal esophagus and distal pylorus. Sham surgery consisted of opening the abdomen, isolating, and clamping the stomach briefly with forceps, and closing the incision. Mice were fed Diet Gel Boost during the 4 days following surgery and were subsequently returned to HFD for the remainder of the study. Body weight was monitored at least weekly throughout the experiment. Body composition was assessed via NMR (Echo MRI) prior to and weekly after surgery. At 3 weeks post-surgery, mice were fasted for 16 hours, and a glucose tolerance test (GTT) was performed. Blood was taken from the tail vein at week two and by heart puncture at euthanasia at week four, respectively, for complete blood cell (CBC) analysis, and for measurement of bone turnover markers.

2.3 Antibody treatments

Subcutaneous injections of monoclonal antibodies were started one day prior to surgery and for the subsequent four weeks. Sham and VSG mice were administered an isotype control antibody (IgG; 10 mg/kg; every three days; Regeneron Pharmaceuticals, Inc.), or antibodies to sclerostin (Anti-SOST; 10 mg/kg; every three days; Regeneron Pharmaceuticals, Inc.) or G-CSFR (Anti-GCSFR; 50 mg; every two days; CSL Limited) [18]. After excluding mice for perisurgical complications, animal numbers for each group were as follows: Sham+IgG, n=8; VSG+IgG, n=10; Sham+Anti-SOST, n=8; VSG+ Anti-SOST, n=10; Sham+Anti-GSCFR, n=7; VSG+ Anti-GSCFR, n=7.

2.4 Intraperitoneal glucose tolerance test (ipGTT)

Glucose homeostasis was assessed as described previously [19]. Briefly, mice were fasted overnight (~16 hours), and body weight and glucose levels were measured at baseline. Following an intraperitoneal injection of glucose (1g glucose/kg body weight), glucose concentrations in tail vein blood were measured with Bayer Contour test strips at 15, 30, 60, 90 and 120 min time points.

2.5 Measurement of circulating factors

Circulating insulin, procollagen type 1 N-terminal propeptide (P1NP) and C-terminal telopeptide of type 1 collagen (CTX-1) concentrations were determined using Ultra Sensitive Mouse Insulin enzyme-linked immunosorbent assay (ELISA) (90080; Crystal Chem; Elk Grove Village, IL), Rat/mouse P1NP ELISA (AC33F1; Immunodiagnostic Systems Inc; Tyne & Wear; UK), and RatLaps™ (CTX-I) EIA (AC06F1; Immunodiagnostic Systems Inc; Tyne & Wear; UK). Concentrations in serum were measured according to manufacturers' instructions.

2.6 Histology and histomorphometry

Tissue histology was performed essentially as described previously [7]. Briefly, soft tissues were fixed in formalin and embedded in paraffin for sectioning. Tibiae were fixed in paraformaldehyde, decalcified in EDTA for at least two weeks, and fixed post-decalcification with 4% paraformaldehyde. Bone tissues were then embedded in paraffin and sectioned. After staining with hematoxylin and eosin (H&E), soft tissues and bones were imaged with an Olympus BX51 microscope. Non-decalcified femurs were used for plastic sectioning and evaluated with Masson Trichrome Staining. For dynamic studies, calcein (CO857; Sigma-Aldrich; St. Louis, MO) dissolved in 0.02 g/ml sodium bicarbonate with 0.9% saline at 20 mg/kg was injected intraperitoneally nine and two days before sacrifice. Quantification of inter-label width (Ir. L. Wi), mineral apposition rate (MAR), and mineralizing surface (MS) on endocortical and periosteal surfaces of femur was performed with Bioquant Osteo 2014 software on randomized samples by a blinded investigator.

2.7 μCT analysis

Tibiae were placed in a 19-mm diameter specimen holder and were scanned over the entire length of the tibiae using a μCT system (μCT100 Scanco Medical). Scan settings were as follows: voxel size 12 μm, 70 kVp, 114 μA, 0.5 mm AL filter, and integration 500 ms. Density measurements were calibrated to the manufacturer's hydroxyapatite phantom. Analysis was performed using the manufacturer's evaluation software with a threshold of 180 Gy for trabecular bone and 280 Gy for cortical bone.

2.8 Bone marrow lipid quantification via osmium tetroxide staining and μCT

After analyses of bone variables, tibiae were decalcified in 14% EDTA for osmium tetroxide staining using our previously published method [20]. A lower threshold (300 grey-scale units) was used for quantification of proximal tibial regulated BMAT (rBMAT), because density of osmium staining is low due to smaller adipocyte size and number. A threshold of 400 grey-scale units was used for quantification of constitutive BMAT (cBMAT) in distal tibia.

2.9 Mechanical testing: 4-point bending assay

After μCT scanning, femora were kept hydrated in saline-soaked gauze until mechanical testing. Femora were loaded to failure in a servohydraulic four-point testing machine (MTS 858 MiniBionix). The mid-diaphysis was loaded with the posterior surface oriented under tension. A custom MATLAB script was used to calculate stiffness, yield load, yield displacement, ultimate load, failure displacement, post-yield displacement, and energy to failure.

2.10 RNA extraction and quantitative real-time PCR (qPCR)

RNA was extracted from caudal vertebrae after powdering in liquid nitrogen and lysis in RNA STAT-60 reagent in a pre-cooled Dounce homogenizer. Quantitative PCR was performed using an Applied Biosystems QuantStudio 3 qPCR machine (Waltham, MA). Gene expression was calculated based on a cDNA standard curve within each plate and normalized to expression of the geometric mean of housekeeping genes *Hprt* and *Rpl32A*.

2.11 Statistics

Significant differences between groups were assessed using two-way (antibody and surgery) or three-way (antibody, surgery, and time) ANOVA in R using the aov() function with the consideration of interactions between variables, followed by Tukey's HSD (honestly significant difference) *post-hoc* test for pairwise comparisons. All graphical presentations are mean ± SD. For statistical comparisons, a p-value of < 0.05 was considered significant.

3. Results

3.1 Anti-SOST improves glucose homeostasis, but otherwise, neither Anti-SOST nor Anti-GCSFR influences effects of VSG on body composition or metabolism.

Six-week-old C57BL/6J male mice were fed a 60% HFD for eight weeks to induce obesity. One day prior to surgery, sham and VSG mice were subcutaneously administered either control IgG, Anti-SOST, or Anti-GCSFR antibodies. Throughout the rest of the study, IgG and Anti-SOST were injected every three days, whereas Anti-GCSFR was administered every second day (Supplemental Figure 1A). After a three-day post-surgical decline, body weights for sham treatments steadily increased over the subsequent 25 days (Figure 1A). Following VSG, body weight also declined for about three days during recovery from the surgical procedure (Figure 1A); however, VSG groups remained at the nadir, without substantial regain of body weight. Although Anti-SOST may have the greater degree of decline in body weight following surgery (Figure 1A), body weight changes over the course of the experiment and end-point body weights were not influenced by Anti-SOST or Anti-GCSFR treatments (Figure 1B and Supplemental Figure 1B). Reduction of body weight with VSG was mainly attributed to a significant loss of fat mass (Figure 1C), including subcutaneous WAT (sWAT), epididymal WAT (eWAT) and brown adipose tissues (BAT) (Supplemental Figure 1C–1E). A minor and transient reduction in lean mass was observed during the first two weeks (Figure 1D), without significant effects on liver weight (Supplemental Figure 1F). Consistent with our previous studies [7], spleen weights were higher in VSG groups (Supplemental Figure 1G). Of note, VSG in Anti-SOST group also

caused a significant splenomegaly, whereas VSG in Anti-GCSFR group had no significant effects on spleen weight (Supplemental Figure 1G).

As reported previously [7], VSG improves glucose tolerance. Whereas Anti-SOST also improved glucose homeostasis, Anti-GCSFR did not alter glucose tolerance (Figure 1E). Random-fed circulating insulin concentrations were decreased overall in VSG groups, and were significantly reduced by VSG in mice treated with Anti-SOST (Figure 1F), suggesting that these mice might have greater insulin sensitivity. Consistent with this notion, insulin concentrations were lower in *Sost*−/− mice fed either a NCD or HFD [21]. As expected with a reduction of fat mass and adipose tissue weights in VSG groups, the size of white and brown adipocytes was reduced, as was the extent of hepatic steatosis (Figure 1G–1H; Supplemental Figure 1H–1I). However, adipocyte size was not influenced by Anti-SOST or Anti-GCSFR treatments. Overall, these data suggest that Anti-SOST improves insulin sensitivity, and that neither antibody treatments otherwise alters the positive effects of VSG on body composition or metabolism of mice on HFD.

3.2 G-CSF receptor antibody treatment partially eliminates VSG-induced leukocyte elevation and loss of BMAT.

In our previous studies, we observed an elevation of circulating white blood cells (WBC) and neutrophils after VSG [7]. In this study at two- and four-weeks post-surgery, WBC and neutrophils were increased in IgG and Anti-SOST treated VSG mice, but induction of these immune cells was largely blocked by Anti-GCSFR treatment (Figure 2A and 2B; 2D and 2E). VSG decreased circulating lymphocytes in mice at two weeks but not four weeks after surgery (Figure 2C, 2F). As observed previously [7], VSG mice developed anemia two and four weeks after surgery, with decreases in red blood cells (RBC), hemoglobin (HGB) and hematocrit (HCT), with a slight induction of circulating platelets four weeks post-surgery (Supplemental Figure 2A–2H). Elevated neutrophils and reduced RBCs in circulation is consistent with our previous observation that VSG causes expansion of myeloid cells and reduction of erythroid cells in bone marrow [7]. We also confirmed our prior observation [7] that VSG stimulates a remarkable loss of proximal tibial rBMAT and distal tibial cBMAT, respectively, at post-surgery week four (Figure 2G–2J). Whereas Anti-SOST and Anti-GCSFR treatments did not alter rBMAT or cBMAT content in sham animals, Anti-SOST caused further loss of cBMAT content of distal tibiae with VSG, whereas Anti-GCSF showed a trend ($p = 0.13$) towards reducing loss of cBMAT with VSG. Taken together, these data indicate that elevated GCSF following VSG stimulates myelopoiesis, and may play a role in loss of cBMAT depots.

3.3 Anti-SOST increases trabecular and cortical bone in sham mice, but only slightly reduces loss of bone mass and bone strength with VSG.

As expected [7], VSG caused trabecular bone loss in proximal tibiae characterized by decreases in trabecular bone volume fraction (Tb. BV/TV), bone mineral density and trabecular thickness (Tb. Th), and increased trabecular separation (Tb. Sp) (Figure 3A–3E). Although Anti-SOST treatment dramatically elevated trabecular bone volume fraction, mineral density, and thickness in Sham mice, Anti-SOST mice had only slightly more trabecular bone mass following VSG than mice receiving IgG and VSG. Anti-GCSFR

treatment did not influence bone parameters in sham or VSG mice. VSG and Anti-SOST treatments had effects in cortical bone similar to those observed for trabecular bone. Whereas VSG decreased cortical bone area fraction (Ct. BA/TA) and bone mineral density (Ct. BMD), Anti-SOST increased these parameters, and a combination of VSG and Anti-SOST resulted in intermediate cortical bone values, similar to IgG-sham controls (Figure 3F–3H). Anti-GCSFR did not protect tibiae from cortical bone loss with VSG (Figure 3F–3H). Mechanical testing of femoral cortical bone revealed that VSG caused bone fragility characterized by reduced ultimate load, stiffness, and fail load (Figure 3I–3K). Although Anti-SOST administration greatly increased femoral ultimate load, stiffness, and failure load, combination of VSG and Anti-SOST resulted in an intermediate femoral strength, similar to that of IgG-sham controls for ultimate load and stiffness, with no change from IgG-VSG for failure load (Figure 3I–3K).

3.4 Effects of VSG, Anti-SOST, and Anti-GCSFR on mineralization of cortical surfaces.

To further characterize mechanisms for increase of bone mass with Anti-SOST, and loss of bone with VSG, we measured circulating markers of bone homeostasis. Concentrations of P1NP, a bone formation marker, were increased with VSG, but not enough to counterbalance the increase in bone resorption with VSG, as indicated by elevated concentrations of circulating CTX-1, a bone resorption marker (Figure 4A and 4B). Anti-SOST increased circulating concentrations of P1NP in Sham mice, without effects on CTX-1, consistent with elevated trabecular and cortical bone (Figure 3). Although Anti-SOST caused an elevation of P1NP in VSG mice, the increase in CTX-1 and bone turnover observed with VSG resulted in a bone mass intermediate between IgG-VSG and IgG-Anti-SOST (Figure 4A, 4B; Figure 3). Anti-GCSFR treatment did not influence circulating concentrations of P1NP or CTX-1 compared to IgG treatment of sham or VSG mice (Figure 4A and 4B).

To further evaluate mechanisms for how VSG and Anti-SOST cause changes in bone, mid-shaft femurs were used for static and dynamic histomorphometry. Quantification of cortical bone area fraction (BA/TA) and width in 2D by histomorphometry (Figure 4C–4E) confirmed the 3D data from μCT (Figure 3F–3H) that cortical bone mass is reduced by VSG, Anti-SOST elevates cortical bone mass, and VSG and Anti-SOST treatment results in an intermediate bone mass. Anti-GCSFR did not cause changes to cortical bone compared to Sham or VSG mice treated with IgG (Figure 4C–4E). Dynamic histomorphometry showed that neither VSG nor Anti-GCSFR altered bone formation parameters relative to controls (Figure 4F–4L). Whereas Anti-SOST treatment strikingly increased the mineralizing surface of endocortical bone in IgG treated Sham mice, Anti-SOST treatment of VSG mice resulted in an intermediate mineralization perimeter relative to the two treatments individually (Figure 4G–4H). Interestingly, in Anti-SOST sham mice, nearly all the endocortical surface was covered by double-labelling (Ec.dl.Pm), but the endocortical inter-label width (Ec.Ir.L.Wi) and mineral apposition rate (MAR) were not changed (Figure 4I–4L). Whereas a combination of VSG and Anti-SOST treatments had much milder changes in double-labelling surface, these treatments did increase Ec.Ir.L.Wi and MAR, indicating that Anti-SOST treatment works through different mechanisms to increase bone formation in sham versus VSG mice. Although Anti-SOST treatment increased mRNA expression of bone formation markers, *Bglap* (Osteocalcin) and *Alpl* (Alkaline phosphatase), in both sham

and VSG groups, combination of VSG and Anti-SOST had slightly reduced expression compared to Anti-SOST alone. Anti-GCSFR did not influence mRNA expression of these bone formation markers (Figure 4M and 4N).

Anti-SOST increases periosteal bone formation.—We also evaluated treatment effects on periosteal bone formation and found that VSG alone did not influence mineralization parameters (Supplemental Figure 3A–3F). However, Anti-SOST administration increased periosteal bone formation by increasing the mineralizing surface (Supplemental Figure 3A and 3B). Whereas VSG Anti-SOST mice showed a slight diminution of double-labeled mineralization compared to Anti-SOST alone, MAR was similar. Interestingly, Anti-GCSFR treatment alone did not influence bone formation as assessed by dynamic histomorphometry; however, Anti-GCSFR interacted with VSG to cause a dramatic decrease in mineralizing surface, double-labelled surface, and mineral apposition rate (Supplemental Figure 3A–3F). Differences in effects of Anti-GCSFR between endocortical and periosteal surfaces suggest that expression of GSCF receptor in osteoblasts or neighboring cells may differ between endosteum and periosteum.

4. Discussion

VSG is an important component of clinical management of obese patients, and this surgery currently accounts for over 60% of the bariatric procedures performed in the United States (asbms.org). Although VSG causes a 51–70% reduction of excess weight, and improves glucose tolerance and cardiovascular disease risk [22], this therapy also has negative side-effects such as rapid bone loss and elevated risk of fracture [5, 7, 23]. Several mechanisms for bone loss with VSG have been explored, such as adaptation to mechanical unloading, nutritional malabsorption (e.g. calcium, vitamin D, and amino acids), abnormalities in calciotropic hormones, and altered endocrine factors including gut hormones (e.g. GLP, PYY and ghrelin), adipokines (e.g. adiponectin, leptin and visfatin) and the cytokine, G-CSF [2, 5, 7, 24]. Altered bile acids and microbiota might also contribute mechanistically to bone loss following bariatric surgery [25]. In addition, clinical studies suggest that SOST, primarily secreted by osteocytes, is elevated in patients after bariatric surgery and circulating concentrations are correlated with bone loss. SOST binds LRP 4, 5 and 6 and prevents their interaction with WNTs, which are important stimulators of bone formation [8, 9, 26, 27]. Inhibition of SOST with antibodies increases bone mass in animals [28, 29], and humans with osteoporosis [30, 31], and is clinically available as a therapy.

Our experiments demonstrate that Anti-SOST dramatically increases bone mass in sham mice, but only mildly protects against loss of bone observed with VSG. Thus, it appears that elevated SOST is not a primary cause of bone loss following VSG, or perhaps that the stomach is required for effects of Anti-SOST on bone metabolism. Interestingly, Anti-SOST treatment increased bone mineralizing surface in both endosteum and periosteum in sham mice without affecting bone formation rate, whereas under VSG conditions, Anti-SOST mainly stimulated bone formation and mineralization rate in endosteum but not in periosteum. These observations suggest that SOST influences osteoblasts/osteocytes through different mechanisms in sham and VSG mice. There may also be unknown overriding factors or mechanisms that modify effects of Anti-SOST in the periosteum under the VSG

conditions, which may partially explain why Anti-SOST treatment could not fully rescue VSG-caused bone loss.

In addition to inhibiting bone formation, SOST has been reported to be associated with obesity and diabetes [10, 32, 33]. Circulating SOST concentrations were negatively correlated with fasting insulin and HOMA–IR in both young and adult subjects [33–35], and positively correlated with serum glucose, HbA1c and free fatty acids in adults [35]. Consistent with these clinical observations, Kim et al. observed that serum SOST concentrations were increased in HFD, *ob/ob* and *db/db* mouse models [21]. Whereas AAV8-*Sost* overexpression increased fat mass, *Sost*−/− mice had reduced fat mass and adipocyte sizes, and improved glucose metabolism and insulin sensitivity when fed HFD [21]. Moreover, administration of SOST-neutralizing antibody to mice also decreased fat mass and lowered circulating insulin concentrations. In our current study, we used a lower dose than Kim et al. [21] (i.e.10 mg/kg vs 30 mg/kg). Under the conditions of our experiments, Anti-SOST did not affect total fat mass or white adipocyte sizes; however, Anti-SOST improved glucose tolerance and when combined with VSG also decreased random-fed insulin concentrations. In line with our findings, Carbone et al. found that baseline serum concentrations of SOST were negative predictors of worse glycemic recovery after VSG which was assessed by fasting glycemia and HbA1c [36]. Mechanisms by which SOST influences insulin resistance are still unclear, but may involve adipose tissues. As mentioned above, SOST binds LRPs to prevent activation of WNT-signaling pathways. Adipocyte specific-*Lrp4* knockout mice mirrored effects of SOST deficiency, with reductions in adipocyte hypertrophy, blood glucose, insulin and serum fatty acids, and improved glucose and lipid homeostasis [37].

Our prior work indicated that G-CSF is increased in circulation of mice following VSG, and is also transiently elevated in serum of female adolescents after surgery [7]. In mice, raising G-CSF in circulation by ectopic expression of AAV8-GCSF recapitulates many of the effects of VSG on bone and the marrow niche, including reductions in bone mass and BMAT, and stimulation of myelopoiesis. Whereas endogenous G-CSF is required for the effects of VSG on induction of neutrophils and depletion of marrow adiposity, mice deficient for G-CSF still lost bone following VSG. In our current investigation, we found that Anti-GCSFR largely blocks the myeloid expansion and partially reduces constitutive BMAT loss following VSG. This differential effect on myeloid cells and BMAT suggests two possibilities: 1) G-CSF receptor might be differentially expressed between myeloid cells and bone marrow adipocytes, or 2) BMAT loss might be secondary to myeloid cell expansion following VSG. Each bone marrow adipocyte interacts directly and indirectly with over 100 hematopoietic cells [38], suggesting that these adipocytes may serve as energy reservoirs to support hematopoietic cell proliferation and functioning. This notion is supported by our recent study that demonstrated lipolysis of bone marrow adipocytes is required for myelopoiesis in caloric restricted mice [39].

Although Anti-GCSFR does not influence bone loss with VSG, it is interesting that it had different effects on endosteal and periosteal bone in sham vs VSG mice. Anti-GCSFR injections did not alter endocortical bone formation and mineralization, but inhibited periosteal mineralizing surfaces, double-labelled surfaces and bone formation rate following VSG. We speculate that GCSFR might be increased or sensitized in periosteal osteoblasts

by VSG, the mechanisms of which are still unclear. Although a bone phenotype was not observed in *Csf3r*−/− mice, a recent study showed that when SOCS3 was absent in Dmp1^{+} osteocytes, *Csf3r*-deficiency further promoted STAT1/3 signaling in osteocytes, delayed cortical bone maturation and elevated local angiogenesis, bone resorption, and bone formation [40].

G-CSF treatment in healthy adults has been associated with alterations of metabolite profiles, including lipids, amino acids, nucleotides, and their related metabolites [41], though the relevance of these changes to metabolic health is still unclear. Interestingly, the *Csf3* gene encoding G-CSF is induced by saturated fatty acids, and has a SNP rs8078723 that is associated with glucose tolerance and adipose tissue insulin resistance [42]. Full-scale profiling of circulating metabolites or metabolism in Anti-GCSFR treated mice was not performed in our study, but we did not observe significant changes in glucose tolerance or adipose depots.

5. Conclusion

Anti-SOST or Anti-GCSFR act through distinct mechanisms to regulate the biology of bone and marrow niche cells, respectively. Anti-SOST partially improves loss of bone following VSG, whereas Anti-GCSFR diminishes the effects of VSG to expand myeloid cellularity and deplete BMAT.

Supplementary Material

Refer to Web version on PubMed Central for supplementary material.

Acknowledgements

This work was supported by grants or fellowships from the NIH to OAM (R01 DK62876; R24 DK092759; R01 DK126230; R01 AG069795), ZL (1P20GM121301) and RJS (P01DK117821); ZL was supported by a fellowship from the American Diabetes Association (1-18-PDF-087). This research was also supported by Regeneron Pharmaceuticals, the Michigan Diabetes Research Center (P30 DK020572), the Michigan Nutrition and Obesity Center (P30 DK089503), and Pilot & Feasibility grant support and core facilities of the Michigan Integrative Musculoskeletal Health Core Center (P30 AR069620).

Abbreviations:

BMAT	bone marrow adipose tissue
CBC	complete blood cell
CTX-1	C-terminal telopeptide of type 1 collagen
G-CSF	granulocyte-colony stimulating factor
GCSFR	G-CSF receptor
Ir. L. Wi	inter-label width
MAR	mineral apposition rate
MS	mineralizing surface

P1NP	procollagen type 1 N-terminal propeptide
SOST	sclerostin
VSG	vertical sleeve gastrectomy

References

1. le Roux CW, Heneghan HM. Bariatric Surgery for Obesity. Med Clin North Am 2018; 102(1): 165–182. e-pub ahead of print 2017/11/21; doi: 10.1016/j.mcna.2017.08.011 [PubMed: 29156184]
2. Hutch CR, Sandoval D. The Role of GLP-1 in the Metabolic Success of Bariatric Surgery. Endocrinology 2017; 158(12): 4139–4151. e-pub ahead of print 2017/10/19; doi: 10.1210/en.2017-00564 [PubMed: 29040429]
3. Cummings DE, Rubino F. Metabolic surgery for the treatment of type 2 diabetes in obese individuals. Diabetologia 2018; 61(2): 257–264. e-pub ahead of print 2017/12/11; doi: 10.1007/s00125-017-4513-y [PubMed: 29224190]
4. Zhang Q, Chen Y, Li J, Chen D, Cheng Z, Xu S et al. A meta-analysis of the effects of bariatric surgery on fracture risk. Obes Rev 2018; 19(5): 728–736. e-pub ahead of print 2018/01/16; doi: 10.1111/obr.12665 [PubMed: 29334691]
5. Stein EM, Silverberg SJ. Bone loss after bariatric surgery: causes, consequences, and management. Lancet Diabetes Endocrinol 2014; 2(2): 165–174. e-pub ahead of print 2014/03/14; doi: 10.1016/S2213-8587(13)70183-9 [PubMed: 24622720]
6. Schafer AL, Kazakia GJ, Vittinghoff E, Stewart L, Rogers SJ, Kim TY et al. Effects of Gastric Bypass Surgery on Bone Mass and Microarchitecture Occur Early and Particularly Impact Postmenopausal Women. J Bone Miner Res 2017. e-pub ahead of print 2017/12/28; doi: 10.1002/jbmr.3371
7. Li Z, Hardij J, Evers SS, Hutch CR, Choi SM, Shao Y et al. G-CSF partially mediates effects of sleeve gastrectomy on the bone marrow niche. J Clin Invest 2019; 129(6): 2404–2416. e-pub ahead of print 2019/05/08; doi: 10.1172/JCI126173 [PubMed: 31063988]
8. Baron R, Kneissel M. WNT signaling in bone homeostasis and disease: from human mutations to treatments. Nat Med 2013; 19(2): 179–192. e-pub ahead of print 2013/02/08; doi: 10.1038/nm.3074 [PubMed: 23389618]
9. Baron R, Gori F. Targeting WNT signaling in the treatment of osteoporosis. Curr Opin Pharmacol 2018; 40: 134–141. e-pub ahead of print 2018/05/13; doi: 10.1016/j.coph.2018.04.011 [PubMed: 29753194]
10. Aznou A, Meijer R, van Raalte D, den Heijer M, Heijboer A, de Jongh R. Serum sclerostin is negatively associated with insulin sensitivity in obese but not lean women. Endocr Connect 2021; 10(2): 131–138. e-pub ahead of print 2021/01/23; doi: 10.1530/EC-20-0535 [PubMed: 33480863]
11. Wang FS, Wu RW, Lain WS, Tsai TC, Chen YS, Sun YC et al. Sclerostin vaccination mitigates estrogen deficiency induction of bone mass loss and microstructure deterioration. Bone 2018; 112: 24–34. e-pub ahead of print 2018/04/14; doi: 10.1016/j.bone.2018.04.007 [PubMed: 29653294]
12. Kobayakawa T, Suzuki T, Nakano M, Saito M, Miyazaki A, Takahashi J et al. Real-world effects and adverse events of romosozumab in Japanese osteoporotic patients: A prospective cohort study. Bone Rep 2021; 14: 101068. e-pub ahead of print 2021/05/14; doi: 10.1016/j.bonr.2021.101068 [PubMed: 33981812]
13. Lewiecki EM, Blicharski T, Goemaere S, Lippuner K, Meisner PD, Miller PD et al. A Phase III Randomized Placebo-Controlled Trial to Evaluate Efficacy and Safety of Romosozumab in Men With Osteoporosis. J Clin Endocrinol Metab 2018; 103(9): 3183–3193. e-pub ahead of print 2018/06/23; doi: 10.1210/jc.2017-02163 [PubMed: 29931216]
14. Tsourdi E, Lademann F, Ominsky MS, Rijntjes E, Kohrle J, Misof BM et al. Sclerostin Blockade and Zoledronic Acid Improve Bone Mass and Strength in Male Mice With Exogenous Hyperthyroidism. Endocrinology 2017; 158(11): 3765–3777. e-pub ahead of print 2017/10/04; doi: 10.1210/en.2017-00247 [PubMed: 28973221]

15. Brent MB, Bruel A, Thomsen JS. Anti-sclerostin antibodies and abaloparatide have additive effects when used as a countermeasure against disuse osteopenia in female rats. Bone 2022; 160: 116417. e-pub ahead of print 2022/04/11; doi: 10.1016/j.bone.2022.116417 [PubMed: 35398589]

16. McDonald MM, Reagan MR, Youlten SE, Mohanty ST, Seckinger A, Terry RL et al. Inhibiting the osteocyte-specific protein sclerostin increases bone mass and fracture resistance in multiple myeloma. Blood 2017; 129(26): 3452–3464. e-pub ahead of print 2017/05/19; doi: 10.1182/blood-2017-03-773341 [PubMed: 28515094]

17. Toscani D, Bolzoni M, Ferretti M, Palumbo C, Giuliani N. Role of Osteocytes in Myeloma Bone Disease: Anti-sclerostin Antibody as New Therapeutic Strategy. Front Immunol 2018; 9: 2467. e-pub ahead of print 2018/11/10; doi: 10.3389/fimmu.2018.02467 [PubMed: 30410490]

18. Yee CS, Xie L, Hatsell S, Hum N, Murugesh D, Economides AN et al. Sclerostin antibody treatment improves fracture outcomes in a Type I diabetic mouse model. Bone 2016; 82: 122–134. e-pub ahead of print 2015/05/09; doi: 10.1016/j.bone.2015.04.048 [PubMed: 25952969]

19. Bagchi DP, Li Z, Corsa CA, Hardij J, Mori H, Learman BS et al. Wntless regulates lipogenic gene expression in adipocytes and protects against diet-induced metabolic dysfunction. Mol Metab 2020; 39: 100992. e-pub ahead of print 2020/04/24; doi: 10.1016/j.molmet.2020.100992 [PubMed: 32325263]

20. Scheller EL, Troiano N, Vanhoutan JN, Bouxsein MA, Fretz JA, Xi Y et al. Use of osmium tetroxide staining with microcomputerized tomography to visualize and quantify bone marrow adipose tissue in vivo. Methods Enzymol 2014; 537: 123–139. e-pub ahead of print 2014/02/01; doi: 10.1016/B978-0-12-411619-1.00007-0 [PubMed: 24480344]

21. Kim SP, Frey JL, Li Z, Kushwaha P, Zoch ML, Tomlinson RE et al. Sclerostin influences body composition by regulating catabolic and anabolic metabolism in adipocytes. Proc Natl Acad Sci U S A 2017; 114(52): E11238–E11247. e-pub ahead of print 2017/12/13; doi: 10.1073/pnas.1707876115 [PubMed: 29229807]

22. Nguyen NT, Varela JE. Bariatric surgery for obesity and metabolic disorders: state of the art. Nat Rev Gastroenterol Hepatol 2017; 14(3): 160–169. e-pub ahead of print 2016/12/03; doi: 10.1038/nrgastro.2016.170 [PubMed: 27899816]

23. Lu CW, Chang YK, Chang HH, Kuo CS, Huang CT, Hsu CC et al. Fracture Risk After Bariatric Surgery: A 12-Year Nationwide Cohort Study. Medicine (Baltimore) 2015; 94(48): e2087. e-pub ahead of print 2015/12/04; doi: 10.1097/MD.0000000000002087 [PubMed: 26632892]

24. Mele C, Caputo M, Ferrero A, Daffara T, Cavigiolo B, Spadaccini D et al. Bone Response to Weight Loss Following Bariatric Surgery. Front Endocrinol (Lausanne) 2022; 13: 921353. e-pub ahead of print 2022/07/26; doi: 10.3389/fendo.2022.921353 [PubMed: 35873004]

25. Tu J, Wang Y, Jin L, Huang W. Bile acids, gut microbiota and metabolic surgery. Front Endocrinol (Lausanne) 2022; 13: 929530. e-pub ahead of print 2022/09/09; doi: 10.3389/fendo.2022.929530 [PubMed: 36072923]

26. Bennett CN, Ouyang H, Ma YL, Zeng Q, Gerin I, Sousa KM et al. Wnt10b increases postnatal bone formation by enhancing osteoblast differentiation. J Bone Miner Res 2007; 22(12): 1924–1932. e-pub ahead of print 2007/08/22; doi: 10.1359/jbmr.070810 [PubMed: 17708715]

27. Kim JH, Liu X, Wang J, Chen X, Zhang H, Kim SH et al. Wnt signaling in bone formation and its therapeutic potential for bone diseases. Ther Adv Musculoskelet Dis 2013; 5(1): 13–31. e-pub ahead of print 2013/03/22; doi: 10.1177/1759720X12466608 [PubMed: 23514963]

28. Li X, Ominsky MS, Warmington KS, Morony S, Gong J, Cao J et al. Sclerostin antibody treatment increases bone formation, bone mass, and bone strength in a rat model of postmenopausal osteoporosis. J Bone Miner Res 2009; 24(4): 578–588. e-pub ahead of print 2008/12/04; doi: 10.1359/jbmr.081206 [PubMed: 19049336]

29. Li X, Ominsky MS, Villasenor KS, Niu QT, Asuncion FJ, Xia X et al. Sclerostin Antibody Reverses Bone Loss by Increasing Bone Formation and Decreasing Bone Resorption in a Rat Model of Male Osteoporosis. Endocrinology 2018; 159(1): 260–271. e-pub ahead of print 2017/10/27; doi: 10.1210/en.2017-00794 [PubMed: 29069393]

30. McClung MR, Grauer A, Boonen S, Bolognese MA, Brown JP, Diez-Perez A et al. Romosozumab in postmenopausal women with low bone mineral density. N Engl J Med 2014; 370(5): 412–420. e-pub ahead of print 2014/01/03; doi: 10.1056/NEJMoa1305224 [PubMed: 24382002]

31. Fabre S, Funck-Brentano T, Cohen-Solal M. Anti-Sclerostin Antibodies in Osteoporosis and Other Bone Diseases. J Clin Med 2020; 9(11). e-pub ahead of print 2020/10/30; doi: 10.3390/jcm9113439
32. Daniele G, Winnier D, Mari A, Bruder J, Fourcaudot M, Pengou Z et al. Sclerostin and Insulin Resistance in Prediabetes: Evidence of a Cross Talk Between Bone and Glucose Metabolism. Diabetes Care 2015; 38(8): 1509–1517. e-pub ahead of print 2015/06/19; doi: 10.2337/dc14-2989 [PubMed: 26084344]
33. Wedrychowicz A, Sztefko K, Starzyk JB. Sclerostin and its association with insulin resistance in children and adolescents. Bone 2019; 120: 232–238. e-pub ahead of print 2018/07/29; doi: 10.1016/j.bone.2018.07.021 [PubMed: 30055341]
34. Kim SH, Choi YJ, Ahn MB, Cho WK, Cho KS, Jung MH et al. Associations between Sclerostin and Anthropometric and Metabolic Parameters in Children and Adolescents. Children (Basel) 2021; 8(9). e-pub ahead of print 2021/09/29; doi: 10.3390/children8090788
35. Singh PK, Naithani M, Pathania M, Mirza AA, Saha S. An Insight Into the Association of Sclerostin With Insulin Sensitivity and Glycemic Parameters in Male Indian Prediabetic and Diabetic Population. Cureus 2022; 14(7): e27123. e-pub ahead of print 2022/08/26; doi: 10.7759/cureus.27123 [PubMed: 36004027]
36. Carbone F, Nulli Migliola E, Bonaventura A, Vecchie A, De Vuono S, Ricci MA et al. Circulating Levels of Sclerostin Predict Glycemic Improvement after Sleeve Gastrectomy. Nutrients 2021; 13(2). e-pub ahead of print 2021/03/07; doi: 10.3390/nu13020623
37. Kim SP, Da H, Li Z, Kushwaha P, Beil C, Mei L et al. Lrp4 expression by adipocytes and osteoblasts differentially impacts sclerostin's endocrine effects on body composition and glucose metabolism. J Biol Chem 2019; 294(17): 6899–6911. e-pub ahead of print 2019/03/08; doi: 10.1074/jbc.RA118.006769 [PubMed: 30842262]
38. Robles H, Park S, Joens MS, Fitzpatrick JAJ, Craft CS, Scheller EL. Characterization of the bone marrow adipocyte niche with three-dimensional electron microscopy. Bone 2019; 118: 89–98. e-pub ahead of print 2018/01/26; doi: 10.1016/j.bone.2018.01.020 [PubMed: 29366839]
39. Li Z, Bowers E, Zhu J, Yu H, Hardij J, Bagchi DP et al. Lipolysis of bone marrow adipocytes is required to fuel bone and the marrow niche during energy deficits. Elife 2022; 11. e-pub ahead of print 2022/06/23; doi: 10.7554/eLife.78496
40. Isojima T, Walker EC, Poulton IJ, McGregor NE, Wicks IP, Gooi JH et al. G-CSF Receptor Deletion Amplifies Cortical Bone Dysfunction in Mice With STAT3 Hyperactivation in Osteocytes. J Bone Miner Res 2022; 37(10): 1876–1890. e-pub ahead of print 2022/07/21; doi: 10.1002/jbmr.4654 [PubMed: 35856245]
41. Hatfield KJ, Melve GK, Bruserud O. Granulocyte colony-stimulating factor alters the systemic metabolomic profile in healthy donors. Metabolomics 2017; 13(1): 2. e-pub ahead of print 2016/12/17; doi: 10.1007/s11306-016-1139-x [PubMed: 27980502]
42. Ordelheide AM, Gommer N, Bohm A, Hermann C, Thielker I, Machicao F et al. Granulocyte colony-stimulating factor (G-CSF): A saturated fatty acid-induced myokine with insulin-desensitizing properties in humans. Mol Metab 2016; 5(4): 305–316. e-pub ahead of print 2016/04/14; doi: 10.1016/j.molmet.2016.02.001 [PubMed: 27069870]

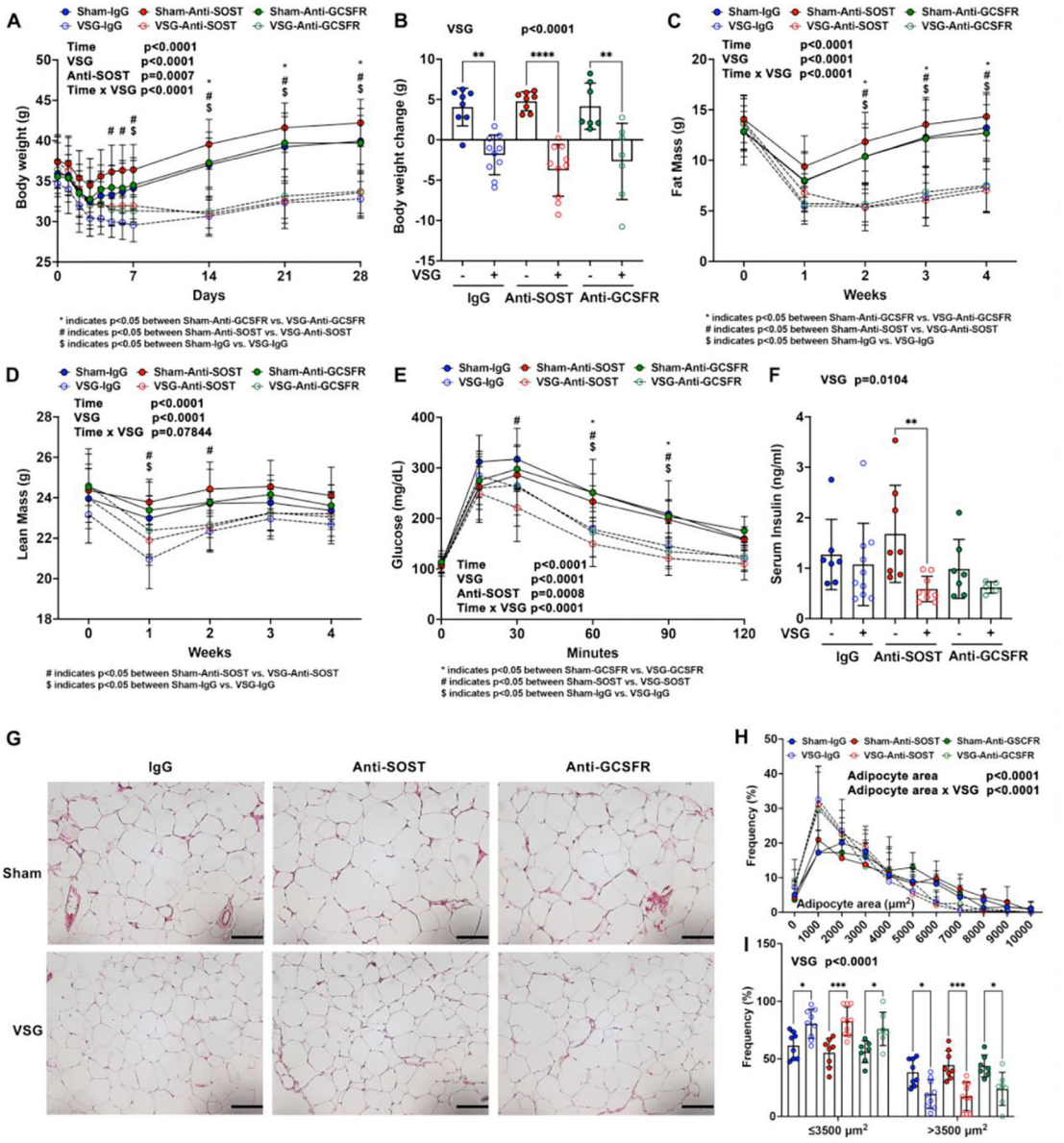

Figure 1. Anti-SOST improves glucose homeostasis, but otherwise, neither Anti-SOST nor Anti-GCSFR influences effects of VSG on body composition or metabolism.

C57BL/6J male mice at six weeks of age were fed a 60% HFD for eight weeks prior to surgery, and for another four weeks after surgery. − indicates sham; + indicates VSG.

A. Body weights at the indicated times.

B. Total body weight changes before surgery and four weeks after surgery were calculated.

C-D. Weekly fat and lean masses determined by NMR prior to and after surgery.

E. Glucose tolerance test was performed three weeks after surgery.

F. Random-fed serum insulin concentrations were measured by ELISA at week four.

G. Epididymal white adipose tissue were fixed, paraffin-sectioned, and H&E stained. Photomicroscopy was at 200x magnification. Scale: 100 μm.

H-I. Adipocyte sizes were quantified by MetaMorph software.

*, # and $ indicate $p < 0.05$ with three-way (A, C, D, E and H) ANOVA followed by Tukey's HSD post-hoc test for pairwise comparisons. Comparisons between groups were labeled under each panel. * indicates $p < 0.05$ with two-way (B, F and I) ANOVA analyses followed by Tukey's HSD multiple comparisons test. Significant effects of VSG, time, antibody treatments, or their interactions are shown.

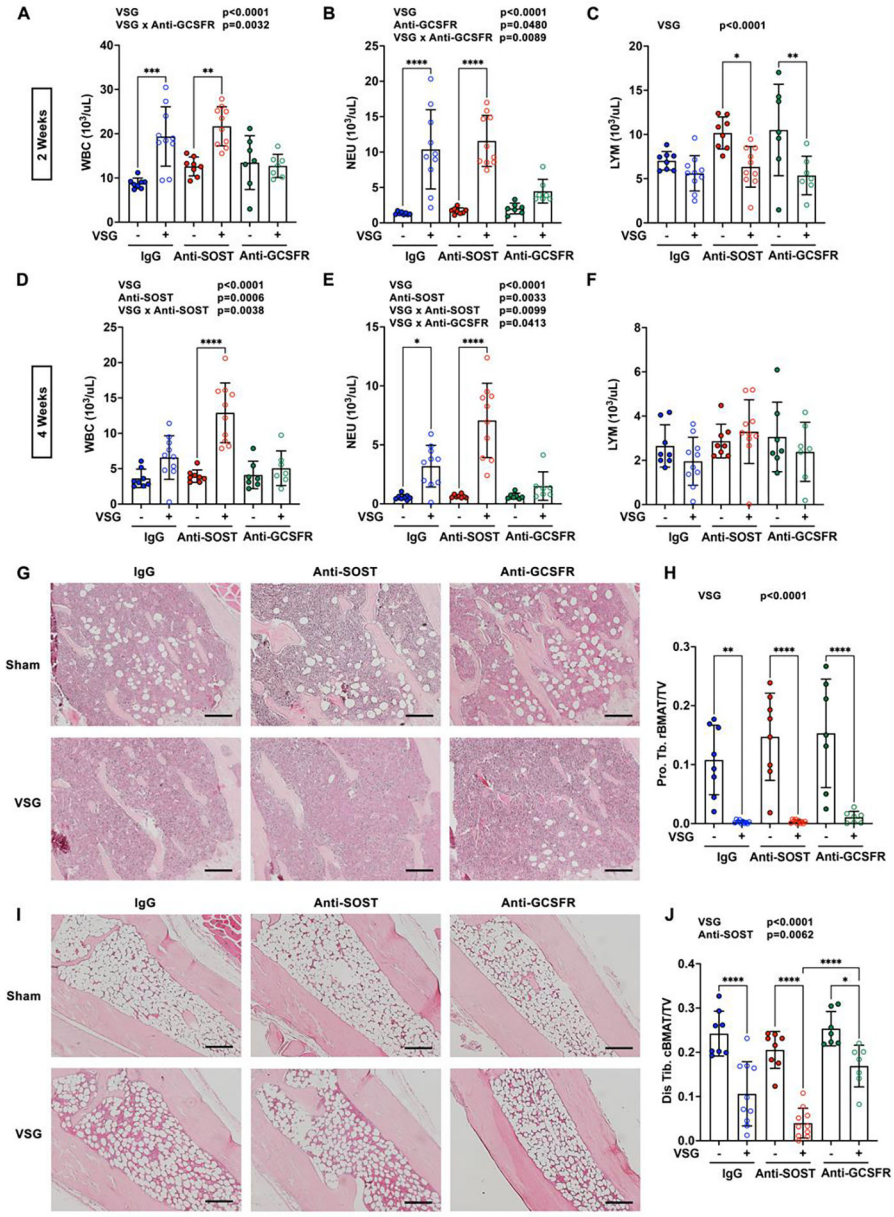

Figure 2. Anti-GCSFR partially eliminates VSG-induced leukocyte elevation and loss of cBMAT.

Obese C57BL/6J male mice underwent sham or VSG surgery and treated with antibodies throughout four weeks after surgery. − indicates sham; + indicates VSG.

A-F. Whole blood was collected for complete blood count (CBC) two and four weeks after surgery. White blood cell (WBC), neutrophils (NEU) and lymphocyte (LYM) numbers were determined.

G and I. Tibiae were decalcified, paraffin-sectioned, and H&E stained four weeks after surgery. Proximal (G) and distal tibiae (I) photomicrographs were taken at 100X magnification. Scale: 200 μm.

H and J. Decalcified tibiae were stained with osmium tetroxide and scanned by μCT. Proximal (Pro. Tb. rBMAT) and distal tibial BMAT (Dis. Tb. cBMAT) were quantified and normalized to total bone volume (TV).

* indicates $p < 0.05$ with two-way ANOVA analyses followed by Tukey's HSD multiple comparisons test. Significant effects of VSG, antibody treatments, or their interactions (VSG x Anti-SOST, VSG x Anti-GCSFR) are shown.

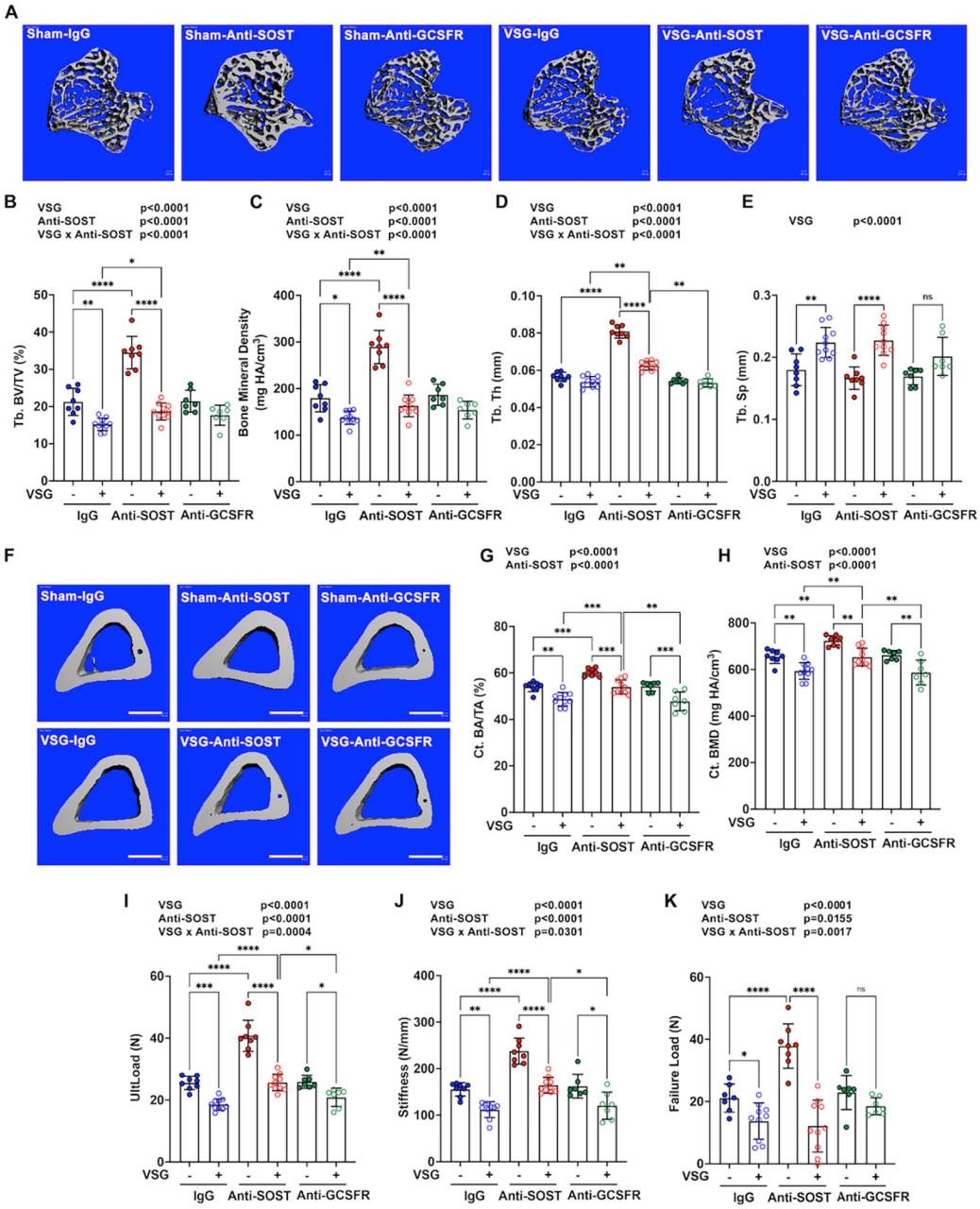

Figure 3. Anti-SOST increases trabecular and cortical bone in sham mice, but only slightly reduces loss of bone mass and bone strength with VSG.

Obese C57BL/6J male mice underwent sham or VSG surgery and were treated with antibodies for the four weeks after surgery. Tibiae were collected for μCT scanning. − indicates sham; + indicates VSG.

A. Representative 3D images of trabecular bone in proximal tibiae. Scale: 500 μm.

B-D. Quantification of trabecular bone (Tb.) variables, including bone volume fraction (BV/TV), mineral density, trabecular thickness (Th) and separation (Sp) was performed.

F. Representative 3D images of cortical bone in mid-shaft tibiae. Scale: 500 μm.

G-H. Cortical bone (Ct.) area fraction (BA/TA) and mineral density (BMD) were measured by μCT.

I-K. Fresh femoral bone tissues were used for the four-point bending assay, in which ultimate load (UltLoad), stiffness and failure load were determined.

* indicates $p < 0.05$ with two-way ANOVA analyses followed by Tukey's HSD multiple comparisons test. Significant effects of VSG, antibody treatments, or their interactions (VSG x Anti-SOST) are shown. No significant interaction between VSG and Anti-GCSFR was detected.

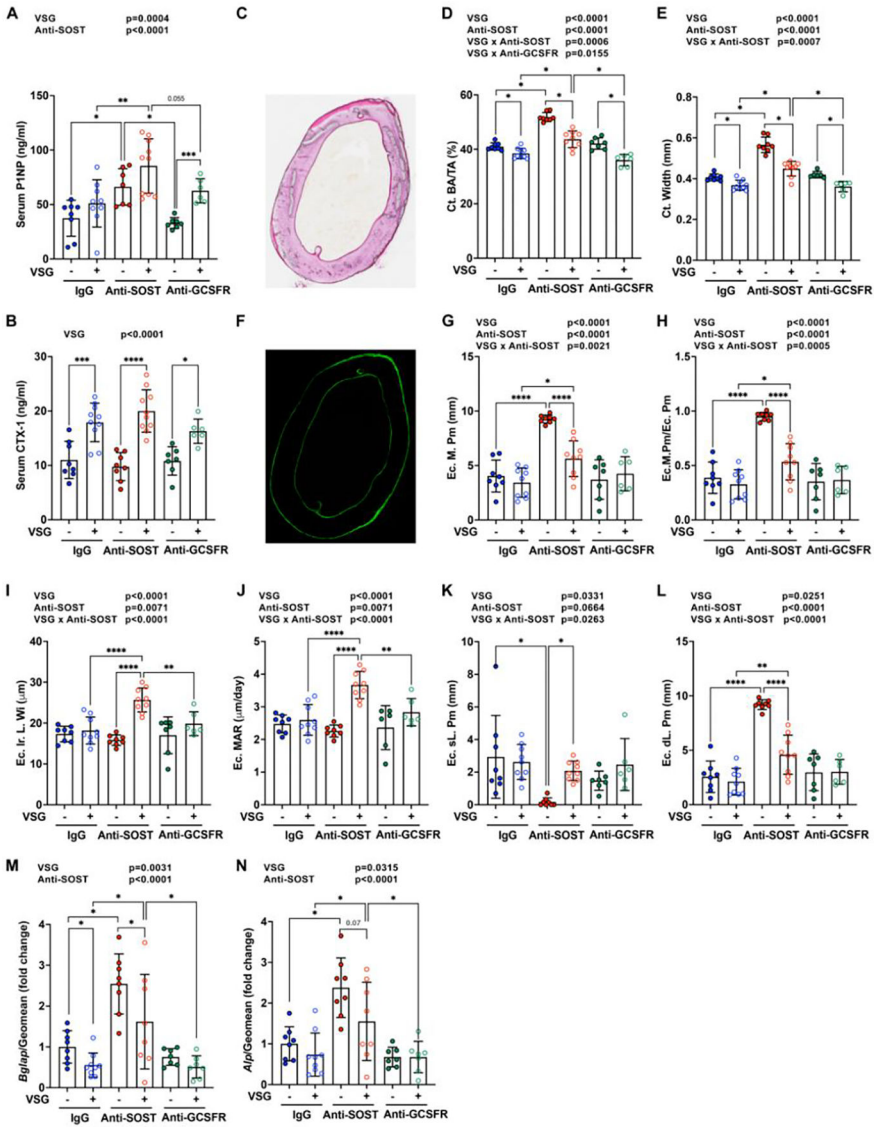

Figure 4. Effects of VSG, Anti-SOST, and Anti-GCSFR on mineralization of cortical surfaces.

Obese C57BL/6J male mice underwent sham or VSG surgery and were treated with antibodies for four weeks after surgery. Serum and femurs were collected. − indicates sham; + indicates VSG.

A-B. Circulating bone turnover makers for bone formation (P1NP) and bone resorption (CTX-1) were measured by ELISAs.

C-L. Calcein injections were performed at nine and two days prior to euthanization. Femurs were collected for plastic sectioning.

C-E. Cross-sections of femurs were used for Goldner's Trichrome staining. Bone area fraction and cortical bone thickness were quantified by BioQuant software.

F-L. Cross-sections of femurs were scanned under a fluorescent microscope. Double-labelled and single-labelled bone surfaces in endosteum were calculated. Ec. M. Pm: Endocortical mineralizing perimeter; Ec. M. Pm/Ec. Pm: Endocortical mineralizing perimeter/ endocortical perimeter; Ec. Ir. Wi: Endocortical interlabel width; Ec. MAR:

Endocortical mineralizing apposition rate; Ec. sL. Pm: Endocortical single-labelled perimeter; Ec. dL. Pm: Endocortical double-labelled perimeter.

M-N. The 4^{th}-6^{th} caudal vertebrae were collected for mRNA purification and qPCR analysis. Gene expression was normalized by geomean of *Hprt* and *Rpl32a*.

* indicates $p < 0.05$ with two-way ANOVA analyses followed by Tukey's HSD multiple comparisons test. Significant effects of VSG, antibody treatments, or their interactions (VSG x Anti-SOST, VSG x Anti-GCSFR) are shown.